The effects of rapid mitochondrial gene loss on organellar proteomes

Jessica M. Warren[1,2], Amanda K. Broz[3], Ryan Stikeleather[1], Daniel B. Sloan[3,*]

[1]Biodesign Institute and School of Life Sciences, Arizona State University, Tempe, AZ, USA
[2]Howard Hughes Medical Institute, Chevy Chase, MD, USA
[3]Department of Biology, Colorado State University, Fort Collins, CO, USA

*Corresponding author: E-mail: dan.sloan@colostate.edu

Abstract

Mitochondrial genomes retain only a tiny number of genes from their bacterial progenitors, including key components of protein translation machinery. The set of mitochondrially encoded tRNAs and ribosomal subunits is highly variable across angiosperms, with many examples of mitochondrial gene loss, replacement, and/or transfer to the nucleus. This dynamic history suggests large-scale remodeling of mitochondrial translation machinery in some lineages, but such conclusions are largely inferred from genomic sequence and protein targeting predictions. Here, we use proteomic (LC-MS/MS) analysis of purified mitochondria and chloroplasts from angiosperm species with major differences in mitochondrial gene content (*Arabidopsis thaliana* and *Silene conica*). Our analysis largely confirms the current understanding of subcellular localization for nuclear-encoded proteins involved in tRNA metabolism and ribosome function in *A. thaliana*, although some aminoacyl-tRNA synthetases (aaRSs) may have more specialized subcellular roles than previously thought. In contrast, *S. conica* has undergone extensive mitochondrial gene loss and numerous associated changes in the composition of its mitochondrial proteome, including retargeting of aaRSs, replacement of ribosomal subunits, and loss of the glutamine amidotransferase (GatCAB) complex. Overall, this analysis illustrates how the complex network of molecular interactions necessary for mitochondrial translation are perturbed by gene loss, transfer, and replacement.

Introduction

Endosymbiotically derived organelles such as mitochondria and plastids evolved from free-living bacteria and still retain their own genomes after more than a billion years (Gould et al. 2008; Roger et al. 2017). Thus, protein synthesis occurs within each of these organelles, using machinery that is distinct from the translation system responsible for synthesizing nuclear-encoded proteins in the cytosol. One common theme in the evolution of obligate endosymbionts is extensive gene loss, functional replacement, and/or transfer to the nucleus (McCutcheon and Moran 2012; Sloan et al. 2018). As such, the gene content in ancient endosymbionts/organelles is whittled down to mostly just key components of the metabolic and biosynthetic functions they provide to the host cell, such as cellular respiration in mitochondria and photosynthesis in plastids. However, even the most ancient endosymbionts/organelles retain some of the genes involved in translation, including ribosomal rRNAs (rRNAs), ribosomal protein subunits, and/or transfer RNAs (tRNAs) (Timmis et al. 2004; Salinas-Giegé et al. 2015; McCutcheon et al. 2024).

Mitochondrial gene content has largely stabilized in some eukaryotic lineages. For example, most bilaterian animals retain the same set of 37 genes that were ancestrally present prior to the Cambrian Explosion (Boore 1999). In contrast, mitochondrial gene content is highly dynamic in angiosperms, often differing even among closely related species (Adams, Qiu, et al. 2002). Angiosperm mitochondrial genomes (mitogenomes) can contain anywhere from 19 to 41 protein-coding genes and from 1 to 19 types of tRNA genes (excluding gene duplicates) (Richardson et al. 2013; Skippington et al. 2015; Yu et al. 2025).

Multiple evolutionary process can facilitate the loss of genes from the mitogenome. Recent losses of mitochondrial protein-coding genes in angiosperms are typically associated with transfer of those genes to the nucleus. Prior to the loss of the native mitochondrial gene copy, the transferred nuclear copy must be expressed, and the resulting protein must be imported back into the mitochondria (Adams et al. 1999; Sloan et al. 2018). In addition to mitochondrial-to-nuclear gene transfer, there are also cases where mitochondrial protein-coding genes are functionally replaced by homologs of plastid or nuclear origin (Adams, Daley, et al. 2002). Losses of mitochondrial tRNA genes appear to follow this latter route. Specifically, they are replaced by import of existing nuclear-encoded tRNAs from the cytosol (Salinas-Giegé et al. 2015; Warren et al. 2021). To our knowledge, there are no documented cases in which a mitochondrial tRNA gene was functionally transferred to the nucleus and targeted back for import into the mitochondria (although one example of plastid tRNA gene transfer was recently discovered in the lycophyte *Selaginella*; Berrissou et al. 2024).

A fundamental challenge in the field of cytonuclear coevolution is to understand the process by which functional gene replacements occur and whether they perturb the intimate and coevolved interactions among gene products encoded in two different genomes. For example, tRNAs must be

53 recognized by their cognate aminoacyl-tRNA synthetases (aaRSs) to be charged with the correct amino
54 acid, and ribosomal proteins and rRNAs physically interact with dozens of subunits within a massive
55 enzyme complex. It is remarkable that functional replacement of a (bacterial-like) mitochondrial gene with
56 its (archaeal-like) nuclear counterpart is possible given that their divergence spans the very deepest split in
57 the tree of life and that even small sequence changes have the potential to disrupt these coevolved
58 interactions (Meiklejohn et al. 2013; Sloan et al. 2023).
59 The mitogenomes found in the angiosperm genus *Silene* are highly variable among species and
60 characterized by many unusual features. Perhaps the most extreme is found in *S. conica*. It has a highly
61 accelerated mutation rate, the largest size of any known angiosperm mitogenome (>11 Mb), and a
62 fragmented multichromosomal structure (Sloan, Alverson, Chuckalovcak, et al. 2012; Broz et al. 2021).
63 Despite its large size, the *S. conica* mitogenome has an unusually small gene content with just 25 protein-
64 coding, 3 rRNA, and 2 tRNA genes (excluding gene duplicates). The near-complete loss of tRNA genes from
65 this mitogenome has been accompanied by extensive import of cytosolic-like tRNA counterparts (Warren
66 et al. 2021). Our previous analysis based on *in silico* targeting predictions and fluorescence microscopy
67 indicated that these tRNA replacement events in *S. conica* have had differing effects on coevolved
68 relationships with aaRSs (Warren et al. 2023). All plant aaRSs are nuclear-encoded, but they differ in where
69 they are localized within the cell. One of the most common patterns is that the plant expresses two aaRSs
70 for a given amino acid – one that functions in the cytosol and another that is dual-targeted and imported
71 into both the mitochondria and plastids (Duchêne et al. 2005). For half of the replaced tRNA genes in *S.*
72 *conica*, we found evidence that a corresponding cytosolic aaRS also gained targeting to the mitochondria.
73 Therefore, the ancestral pairing of a cytosolic tRNA and aaRS was apparently maintained in these cases
74 and simply relocated to an additional cellular compartment. In contrast, we did not find evidence of aaRS
75 retargeting for the other half of replaced tRNA genes, suggesting that (bacterial-like) organellar aaRSs are
76 responsible for charging the cytosolic-like tRNAs now being imported into the mitochondria. However,
77 these inferences have not been investigated by direct analysis of mitochondrial protein content, as the
78 mitochondrial proteome of *S. conica* remains entirely unexplored.
79 Here, we perform proteomic analysis of *S. conica* and the model angiosperm *Arabidopsis thaliana*
80 using liquid chromatography-tandem mass spectrometry (LC-MS/MS). The resulting datasets allow us to
81 directly investigate how the composition of the mitochondrial proteome and its translational machinery
82 have changed in association with the extensive gene loss from the *S. conica* mitogenome.
83
84 **Results and Discussion**
85
86 *Purification of mitochondrial and chloroplast proteomes*

87 We analyzed LC-MS/MS data from extracted protein content from two biological replicates of purified
88 mitochondria, purified chloroplasts, and total leaf tissue from both *A. thaliana* and *S. conica*. A similar
89 dataset was also generated for a third species (*Agrostemma githago*). However, preliminary analysis of the
90 *A. githago* dataset indicated that it had limited detection of the translation machinery that was the focus of
91 this study. Therefore, we have deposited data from all three species (see Data Availability), but only *A.*
92 *thaliana* and *S. conica* were analyzed in the present study.

93 We used peptide-spectrum matches (PSMs) as a semi-quantitative metric of protein abundance.
94 Overall, we detected PSMs from 5599 and 5491different proteins in *A. thaliana* and *S. conica*, respectively
95 (Table 1). To verify the efficacy of our organelle purifications, we measured the enrichment of each
96 mitochondrial-encoded and plastid-encoded protein in the purified organelles relative to total leaf tissue
97 based on PSM counts. Although we did detect PSMs for mitochondrial-encoded proteins in chloroplast
98 samples and vice versa, we observed a strong quantitative difference between the sample types that
99 confirmed we had effectively enriched for mitochondrial and chloroplast subcellular fractions (Figure 1).
100 We also found this same pattern of strong enrichment using ion intensity (i.e., peak area) as a measure of
101 protein abundance instead of PSM counts (Figure S1).

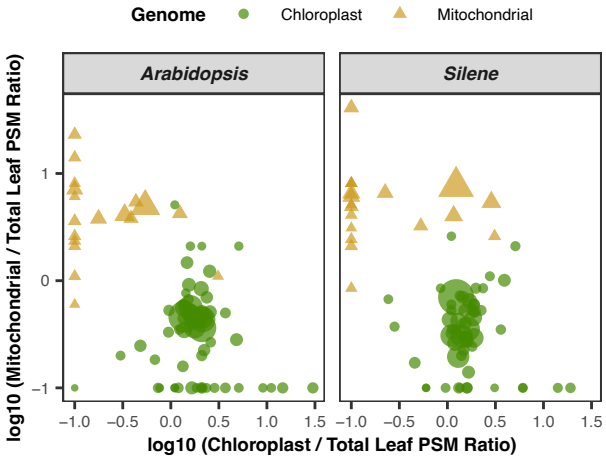

Figure 1. Enrichment of proteins encoded by the organellar genomes in purified chloroplast fractions (x-axis) and mitochondrial fractions (y-axis). Enrichment ratios are quantified based on summed counts of PSMs from two replicates relative to counts in leaf tissue samples. Each point represents a protein, and point sizes are scaled proportionally to the total number of PSMs observed for the corresponding protein across all samples. Plastid-encoded proteins and mitochondrial-encoded proteins are represented by green circles and gold triangles, respectively.

102 *Subcellular specialization of Arabidopsis aaRSs*

103 Numerous studies have been conducted to catalog the subcellular localization of aaRSs in *A. thaliana*,
104 primarily by fusing putative organelle-targeting transit peptides from aaRSs to fluorescent proteins or other
105 reporters, which could be visualized within cells or tested for import into isolated organelles *in vitro*
106 (Mireau et al. 1996; Uwer et al. 1998; Souciet et al. 1999; Peeters et al. 2000; Duchêne et al. 2001; Duchêne

107 et al. 2005). Collectively, these studies established a consensus for the subcellular localization of all
108 aaRSs in *A. thaliana* (Table 2), which we will refer to as the Duchêne classification because the most
109 extensive sampling was performed by Duchêne et al. (2005), and the cumulative body of work was later
110 summarized by Duchêne et al. (2009). For most amino acids, *A. thaliana* expresses two different aaRSs –
111 one that is targeted to the cytosol (cyto-only) and another that is dual-targeted to both the chloroplasts
112 and mitochondria (chloro-mito). However, some aaRSs exhibit atypical patterns of subcellular
113 localization, such as dual targeting to both the cytosol and mitochondria (cyto-mito) or to all three cellular
114 compartments (Duchêne et al. 2009). One LeuRS enzyme (AT4G04350) was also found to be specific to the
115 chloroplasts (chloro-only).

116 Overall, our patterns of aaRS enrichment in mitochondrial and chloroplast fractions strongly
117 aligned with the Duchêne classification (Figure 2; Table 2). All aaRSs that had been previously described as
118 cyto-only showed little or no detection in our purified mitochondrial and chloroplasts samples from *A.*
119 *thaliana*. In contrast, all of these aaRSs were detected in total leaf tissue (except for four that presumably
120 had low overall expression due to the presence of close paralogs with higher expression; Table 2),
121 supporting the inference that their functional role is limited to the cytosol. Likewise, the four aaRSs
122 previously identified cyto-mito aaRSs (GlyRS, LeuRS, ValRS, ThrRS) were found at higher abundance in
123 mitochondria than all the cyto-only aaRSs and were not detected in chloroplasts. As expected, previously
124 identified chloro-mito aaRSs were generally detected at high abundance in both organelle fractions, and
125 the chloro-only LeuRS was found in high abundance in our chloroplast fractions but not detected in
126 mitochondria (Figure 2; Table 2). In addition, our data support previous inferences that one ArgRS enzyme
127 (AT4G26300) functions in all three cellular compartments. In prior GFP localization studies, this ArgRS
128 protein was only observed to be targeted to the chloroplasts (Duchêne et al. 2005), but it was predicted to
129 function in the cytosol and mitochondria as well because mutants lacking the only other known *A. thaliana*
130 ArgRS gene (AT1G66530) are still viable (Berg et al. 2005; Duchêne et al. 2009). Indeed, we detected
131 AT4G26300 in both mitochondrial and chloroplast fractions (Figure 2). In contrast, AT1G66530 was only
132 detected in total leaf samples and at very low abundance (only a single PSM in each replicate sample).
133 Therefore, it is likely that both ArgRS enzymes are expressed in the cytosol, but whether AT1G66530 makes
134 any contribution to cytosolic translation is not clear.

135 Despite the overall congruence between our proteomic analysis and the Duchêne classification,
136 there were some discrepancies that point to potential refinements in our current understanding of aaRS
137 targeting in *A. thaliana* (Table 2). First, a previous analysis has indicated that there is one chloro-mito AlaRS
138 (AT5G22800) and another AlaRS (AT1G50200) targeted to all three cellular compartments (Duchêne et al.
139 2005). However, we did not detect AT1G50200 in purified chloroplasts, and we did not detect AT5G22800
140 in purified mitochondria (Figure 2). Therefore, it is possible that AlaRSs follow a division of labor similar to

141 the pattern observed for LeuRSs, with distinct cyto-mito and chloro-only enzymes. This scenario would be
142 consistent with the finding that plastid tRNA-Ala is a poor substrate for the cytosolic AlaRS in spinach
143 (Steinmetz and Weil 1986) and that the fusion of the AT1G50200 transit peptide to β-glucuronidase (GUS)
144 failed to localize reporter activity to chloroplasts (Mireau et al. 1996). However, it is difficult to reconcile
145 with the lines of evidence supporting dual-organellar localization of both AlaRSs reported by Duchêne et
146 al. (2005), so it is possible that AT1G50200 and AT5G22800 are indeed present in chloroplasts and
147 mitochondria, respectively, but at levels we were unable to detect with our analysis.
148 Second, the ThrRS enzymes might offer yet another example of division of labor between cyto-mito
149 and chloro-only enzymes in *A. thaliana*, even though previous analysis has suggested two different ThrRSs
150 functioning in the mitochondria (one chloro-mito and one cyto-mito). Fusion of the transit peptide from the
151 putative chloro-mito ThrRS (AT2G04842) to reporter genes was previously shown to drive localization and
152 import into both chloroplasts and mitochondria (Duchêne et al. 2005), but we only detected this ThrRS in
153 chloroplasts. As expected, we did not detect the previously classified cyto-mito ThrRS (AT5G26830) in
154 chloroplasts. A third ThrRS gene (AT1G17960) has been identified in *A. thaliana* and presumed to have
155 cyto-only function due to the apparent lack of any transit peptide (Duchêne et al. 2005), but we did not
156 detect this protein in any of our samples.
157 Third, our results may provide insights into the unusual cases of GlyRS and ValRS function in *A.*
158 *thaliana*. Although there is a cyto-mito and a chloro-mito aaRS reported in each case, the cyto-mito aaRS
159 has been suggested to not function in aminoacylation within the mitochondria for both Gly (Duchêne et al.
160 2001) and Val according to a personal communication reported by Duchêne et al (2009). We detected the
161 chloro-mito GlyRS (AT3G48110) at substantial abundance in mitochondria (Figure 2), supporting the earlier
162 interpretation that it could be the sole or primary enzyme responsible for aminoacylation of mitochondrial
163 tRNA-Gly even though the cyto-mito GlyRS (AT1G29880) is also present in the mitochondrial fraction. In
164 contrast, we detected the putative chloro-mito ValRS (AT5G16715) at only very low abundance in *A.*
165 *thaliana* mitochondria (only a single PSM in one of the two replicate samples; Figure 2). Coupled with the
166 fact that there has been conflicting or inconsistent evidence for targeting of AT5G16715 to mitochondria
167 (Duchêne et al. 2005; Duchêne et al. 2009), this observation raises the possibility that ValRS represents a
168 fourth example (along with AlaRS, LeuRS, and ThrRS) where the division of labor is primarily between a
169 cyto-mito and a chloro-only enzyme.

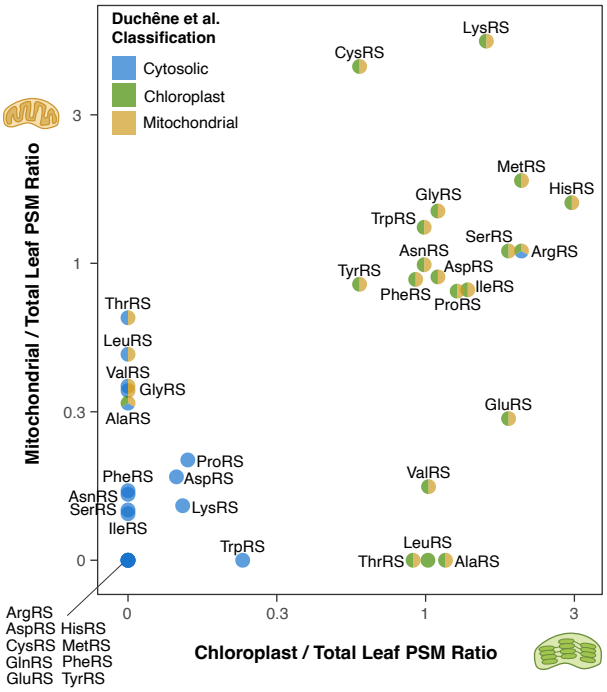

Figure 2. Summary of mitochondrial and chloroplast enrichment of *Arabidopsis thaliana* aaRSs relative to total leaf samples based on ratios of PSM counts combined across two biological replicates. Color coding of points reflects whether the aaRS was previously classified as being targeted to the cytosol, chloroplasts, and/or mitochondria (Duchêne et al. 2005; Duchêne et al. 2009).

Changes in aaRS targeting and tRNA interactions associated with massive mitochondrial tRNA gene loss in Silene conica

With only two tRNA genes (tRNA-Ile and tRNA-fMet), the *S. conica* mitogenome represents one of the most extreme cases of mitochondrial tRNA gene loss in plants (Sloan, Alverson, Chuckalovcak, et al. 2012), with potential widespread effects on aaRS-tRNA interactions. Only six of the 20 aaRS types are not expected to be affected by recent mitochondrial tRNA gene loss in the *Silene* lineage – either because *S. conica* has retained the corresponding tRNA gene in its mitochondrial genome (IleRS) or because the corresponding tRNA gene had already been lost prior to the most recent common ancestor of angiosperms (AlaRS, ArgRS, LeuRS, ThrRS, and ValRS). Note that even though the *S. conica* mitogenome retains a gene for the initiator tRNA-fMet, it has lost the elongator tRNA-Met gene, so interactions involving MetRS may still have been perturbed. For four of these six aaRS types (AlaRS, ArgRS, IleRS, and LeuRS), mitochondria from *A. thaliana* and *S. conica* exhibit the same bias with respect to cytosolic-like vs. organellar-like aaRSs (Figure 3). However, the bias towards cytosolic-like ThrRS and ValRS in *A. thaliana* mitochondria (see preceding section) is not shared by *S. conica*. In these cases, it is likely that *S. conica* has retained the ancestral state (an organellar-like aaRS in the mitochondria) and that the *Arabidopsis* lineage has evolved to import a cytosolic-like enzyme.

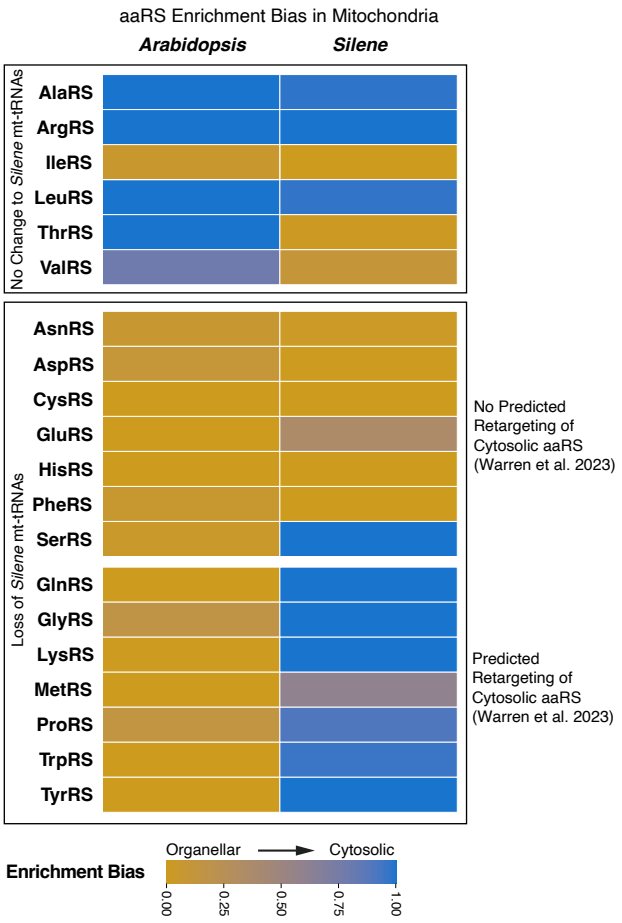

Figure 3. Summary of whether mitochondrial samples were biased towards containing organellar-like vs. cytosolic-like aaRSs based on proteomic analysis. The mitochondrial enrichment bias metric was calculated as described in the Methods. Note that there is no organellar-like GlnRS because mitochondria and plastids use GluRS and the indirect aminoacylation pathway for tRNA-Gln (Pujol et al. 2008). Therefore, enrichment bias for GlnRS was simply reported as "organellar" if the cytosolic-like GlnRS was not detected in mitochondria and cytosolic if the cytosolic-like GlnRS was detected in mitochondria. Overall, the results strongly align with previous predictions (Warren et al. 2023) for which cytosolic aaRSs were or were not retargeted to mitochondria with the exception of SerRS, which showed clear evidence for retargeting despite the lack of any predicted transit peptide.

The other 14 aaRS types are potentially affected by the large-scale loss/replacement of mitochondrial tRNA genes in *S. conica*. Previous analysis based on *in silico* prediction and fusions of putative transit peptides to GFP (Warren et al. 2023) found that a cytosolic-like aaRS likely gained targeting to the mitochondria in seven of these 14 cases (GlnRS, GlyRS, LysRS, MetRS, ProRS, TrpRS, and TyrRS) where a native mitochondrial tRNA gene was replaced by import of its cytosolic counterpart. Proteomic data supported these predictions in all seven cases (Figure 3), indicating that the ancestral pairing of cytosolic-like tRNAs and aaRSs has been preserved and simply retargeted to also function in the mitochondria. Notably, cytosolic-like and organellar-like MetRS enzymes were both detected in *S. conica* mitochondria (Figure 3), likely reflecting the contrasting pattern of loss/replacement of the elongator tRNA-Met gene but retention of the initiator tRNA-fMet gene in the mitogenome (Sloan, Alverson, Chuckalovcak, et al. 2012).

197 The remaining seven aaRS types (AsnRS, AspRS, CysRS, GluRS, HisRS, PheRS, and SerRS) were not
198 previously predicted to show retargeting of the cytosolic-like aaRS in *S. conica* (Warren et al. 2023). Our
199 analysis here generally supported these predictions. However, SerRS was a notable exception, showing
200 clear evidence of retargeting of the cytosolic-like SerRS to the mitochondria (Figure 3). This finding resolves
201 a mystery because previous transit peptide analysis had suggested that the ancestral organellar-like SerRS
202 had lost targeting to mitochondria and was localized exclusively to chloroplasts in the *Silene* lineage,
203 making it unclear which enzyme was providing SerRS function in mitochondria (Warren et al. 2023). Our
204 proteomic results indicate that SerRS represents an eighth case of retargeting a cytosolic-like aaRS to the
205 mitochondria. Our analysis also detected a mix of both organellar-like and cytosolic-like GluRS proteins in
206 *S. conica* mitochondria (Figure 3). It is possible that the cytosolic-like protein is a truncated version of the
207 enzyme that was previously predicted based on full-length mRNA sequencing and *in silico* targeting
208 analysis (Warren et al. 2023). If so, it is not clear whether this protein would have a functional role in
209 aminoacylation in the mitochondria given that it lacks a substantial N-terminal portion (129 amino acids)
210 of the enzyme body.
211
212 *Duplication and subfunctionalization of the organellar PheRS in Silene conica*
213 PheRS is one of the aaRS types that shows no evidence of cytosolic enzyme retargeting despite the loss of
214 the mitochondrial tRNA-Phe and apparent functional replacement with its cytosolic counterpart (Figure 3)
215 (Warren et al. 2023). The persistence of the organellar-like PheRS in *S. conica* mitochondria follows a
216 broader evolutionary pattern, as this aaRS appears to be one of the very last to be functionally replaced in
217 the mitochondria even in cases of complete loss of all tRNA genes from the mitogenome (Pett and Lavrov
218 2015; DeTar et al. 2024). The recalcitrance of the organellar-like PheRS is thought to result from its
219 cytosolic counterpart being divided into two subunits, making it improbable for both subunits to
220 independently gain import into the mitochondria and serve as a viable functional replacement. In the
221 *Silene* lineage, the organellar-like PheRS gene has been duplicated, and fusion of putative transit peptides
222 to GFP suggested that the paralogs have subfunctionalized with one specializing on the mitochondria and
223 the other specializing on the chloroplasts (Warren et al. 2023). Our proteomic analysis supported this
224 subfunctionalization model, as the *S. conica* chloroplast fraction contained only the putative chloroplast
225 specialist, whereas the mitochondrial fraction was dominated by the putative mitochondrial specialist
226 (Figure 4A).
227 The organellar (mitochondrial) PheRS in humans has been found to have the capacity to charge
228 tRNA-Phe substrates from diverse organisms (Klipcan et al. 2012). If plant organellar PheRSs share this
229 capacity, it may have predisposed them to charge imported cytosolic tRNA-Phe in the mitochondria of *S.*
230 *conica*. In addition, the division of labor observed between the two organellar-like PheRSs in *S. conica*

231 could be a response to the challenges associated with a single organellar-like aaRS having to recognize
232 both a cyanobacterial-like tRNA-Phe in chloroplasts and a cytosolic-like tRNA-Phe imported into the
233 mitochondria.

234 To identify amino acid substitutions that might potentially have improved the ability of the *S. conica*
235 mitochondrial PheRS to charge cytosolic tRNA-Phe, we compared the *S. conica* organellar PheRS
236 sequences to each other and to orthologs from a broad sampling of species that represented angiosperms
237 (including eudicots, monocots, magnoliids, and *Amborella*), gymnosperms (*Ginkgo*), bryophytes
238 (*Physcomitrium*), and green algae (*Micromonas* and *Ostreococcus*). The enzyme bodies (i.e., after removal
239 of putative transit peptide sequences) of the *S. conica* mitochondrial and chloroplast PheRSs differed by
240 39 amino acid substitutions (out of 374 positions). Four of the substitutions in the mitochondrial PheRS
241 (I184V, S343T, A363G, and R411I) were at sites that were otherwise universally conserved across our
242 sampling of plant and algal taxa (Figure S2A). No substitutions were found at any such conserved sites in
243 the *S. conica* chloroplast PheRS sequence.

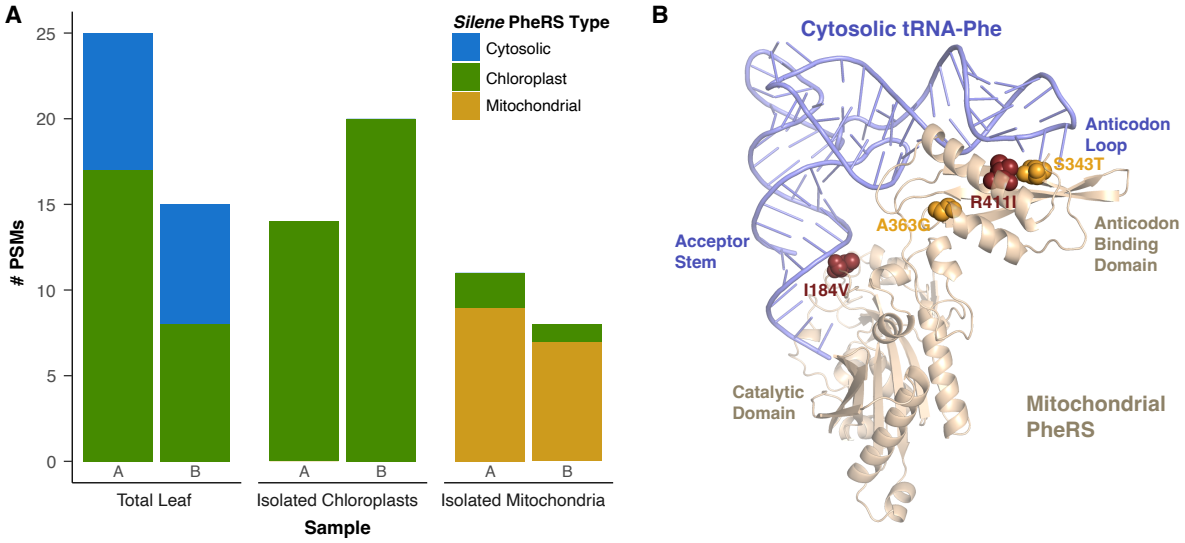

Figure 4. Duplication of organellar PheRS has led to subfunctionalized copies with specialized chloroplast and mitochondrial localization. (A) PSM counts in *Silene conica* samples (with A and B replicates shown separately for each sample type) indicate that the putative chloroplast PheRS was the only one present in the chloroplast fraction, whereas the putative mitochondrial type dominated the mitochondrial fraction, aligning with previous predictions (Warren et al. 2023). (B) AlphaFold3 model of the structural interaction between *S. conica* mitochondrial PheRS and cytosolic tRNA-Phe. Four substitutions at PheRS residues that are otherwise broadly conserved across green plants are labeled and highlighted with "sphere" representation. Two of those substitutions (I184V) and (R411I) are emphasized with a darker color because the exact same substitutions evolved in parallel in another angiosperm (*Sapria himalayana*) with an organellar-like PheRS that is expected to function exclusively in the mitochondria and charge imported cytosolic tRNA-Phe.

244 To further explore the potential relevance of these four substitutions, we compared the PheRS
245 sequence to a representative of the Rafflesiaceae (*Sapria himalayana*) because this family of parasitic
246 (non-photosynthetic) plants has also lost the native tRNA-Phe gene from its mitogenome, and it has lost its
247 plastid genome entirely (Molina et al. 2014; Smith and Asmail 2014; DeTar et al. 2024). Therefore, its

248 organellar PheRS is expected to function exclusively in the mitochondria (due to lack of translation in the
249 plastid) and likely charges imported cytosolic tRNA-Phe. Strikingly, the *S. himalayana* PheRS has
250 independently evolved the exact same amino acid substitutions at two of the four sites identified in the *S.*
251 *conica* mitochondrial PheRS (I184V and R411I; Figure S2A). The R411I substitution is at a residue predicted
252 to interact with the G37 position in cytosolic tRNA-Phe (Figure 4B), which is situated immediately adjacent
253 to the anticodon and represents the only sequence difference in the anticodon loop between cytosolic and
254 mitochondrial tRNA-Phe (Figure S2B). The I184V substitution is at a position abutting the 3′ side of the
255 tRNA-Phe acceptor stem (Figure 4B), which contains multiple nucleotide substitutions that distinguish
256 cytosolic and mitochondrial tRNA-Phe (Figure S2B). We also compared to the organellar PheRS from
257 another parasitic plant (*Balanophora fungosa*) that has lost the mitochondrial tRNA-Phe gene. The *B.*
258 *fungosa* organellar PheRS is expected to function in both the mitochondria and plastids because the
259 Balanophoraceae lineage still retains a plastid genome (Su et al. 2019; Ceriotti et al. 2021). However, this
260 plastid genome has also lost its copy of the tRNA-Phe gene, so the *B. fungosa* organellar PheRS is expected
261 to exclusively charge cytosolic tRNA-Phe. We found that *B. fungosa* PheRS also carried the R411I
262 substitution. It also had a substitution at residue 184, although it was an Ile-to-Thr change rather than the
263 Ile-to-Val substitution observed in *S. conica* and *S. himalayana*.
264 Given the recurrence of substitutions in *S. conica*, *S. himalayana*, and *B. fungosa* at these two sites
265 that are otherwise highly conserved in green plants, we speculate that they are involved in the
266 specialization of these enzymes to charging an imported cytosolic tRNA-Phe substrate. In the *S. conica*
267 lineage, it appears that these substitutions occurred prior to the divergence of multiple *Silene* species that
268 were previously sampled (Warren et al. 2023). However, another member of this family (*Agrostemma*
269 *githago*) shares the organellar PheRS paralogs with *Silene* (Warren et al. 2023), but it does not share these
270 two amino acid substitutions. Because *A. githago* independently lost the mitochondrial tRNA-Phe gene and
271 must use its imported cytosolic counterpart (Warren et al. 2021), the lack of these two substitutions in the
272 *A. githago* mitochondrial PheRS implies that they are not essential for charging cytosolic tRNA-Phe.
273 Likewise, it is possible that other amino acid substitutions distinguishing the *S. conica* mitochondrial and
274 plastid PheRSs might contribute to their specialization on different tRNA substrates even if they are not at
275 positions that are widely conserved in other taxa. Furthermore, it is possible this gene duplication has
276 occurred for reasons that are entirely unrelated to changes in tRNA substrates. Performing aminoacylation
277 assays with recombinantly expressed proteins (Gamper and Hou 2020) would be a promising route to
278 assess the effect of specific substitutions on charging efficiency with different tRNA substrates and to
279 distinguish among these alternative hypotheses.
280
281 *Loss of the GatCAB complex in Silene conica mitochondria*

282 Like most bacteria, plant mitochondria and plastids generally lack GlnRS activity and instead use an
283 indirect pathway in which GluRS indiscriminately charges tRNA-Gln with Glu followed by enzymatic
284 conversion of Glu to Gln by the glutamyl-tRNA amidotransferase enzyme complex (GatCAB) (Pujol et al.
285 2008). In *S. conica*, the loss of the mitochondrial tRNA-Gln gene has been associated with import of
286 cytosolic-like tRNA-Gln and GlnRS into the mitochondria (Figure 2). Therefore, we would predict that
287 GatCAB activity is no longer necessary in *S. conica* mitochondria because they now use the direct Gln
288 aminoacylation pathway typical of cytosolic translation (Rogers and Söll 1995). Our proteomic analysis
289 supported this prediction. All three GatCAB subunits were detected in both the mitochondria and
290 chloroplast fractions from *A. thaliana* but only in the chloroplast fraction from *S. conica* (Table S1).
291 Therefore, the GatCAB complex and the indirect Gln aminoacylation pathway appears to no longer
292 function in *S. conica* mitochondria.
293
294 *Retention of other components of tRNA metabolism machinery in Silene conica mitochondria*
295 The two remaining tRNA genes in the *S. conica* mitogenome (tRNA-fMet and tRNA-Ile) are noteworthy
296 because they both have distinctive bacterial-like features. Bacterial translation is initiated with an N-
297 formylmethionine (fMet), which is synthesized by the methionyl-tRNA formyltransferase (MTF). After tRNA-
298 fMet is initially charged with Met, the MTF enzyme formylates the amino group of the Met residue to
299 produce fMet (Ibba and Söll 2004). Meanwhile, a class of bacterial tRNA-Ile genes have a CAT anticodon,
300 which would typically correspond to an ATG (Met) codon. However, the C base in this anticodon is
301 modified to lysidine by tRNA-Ile lysidine synthetase (TilS), which results in decoding of Ile codons (Suzuki
302 and Miyauchi 2010). Homologs of bacterial MTF and TilS are both found in plant nuclear genomes and
303 expected to function in mitochondrial and plastid translation systems (Warren and Sloan 2020). Given the
304 retention of tRNA-fMet and tRNA-Ile genes in the *S. conica* mitogenome, we would predict that MTF and
305 TilS are also functional in *S. conica* mitochondria. Accordingly, we detected both proteins in the
306 mitochondrial fraction (Table S1). TilS was only supported by a single PSM in one of the *S. conica*
307 mitochondrial samples, which is likely due to low overall expression, as it was not detected in chloroplast
308 or total-leaf samples from *S. conica* or in any *A. thaliana* samples. Nonetheless, the detection of both of
309 these enzymes suggests that the bacterial-like translation features associated with tRNA-fMet and tRNA-
310 Ile have been retained in *S. conica* mitochondria, which contrasts with the functional loss of GatCAB and
311 many aaRSs.
312 Mitochondrial tRNA metabolism also relies on additional enzymes that are typically shared with
313 other subcellular compartments (von Braun et al. 2007; Canino et al. 2009; Gobert et al. 2010; Gutmann et
314 al. 2012; Salinas-Giegé et al. 2015), including those responsible for cleaving primary transcripts to remove
315 5′ ends (protein-only RNase P [PRORP]) or 3′ ends (tRNase Z) and for adding a 3′ CCA tail (CCAse). In

general, we had limited sensitivity to detect these enzymes with our dataset (Table S1). Although we did confirm the expected presence of CCAse in *S. conica* mitochondria, the general lack of signal for PRORP or tRNase Z enzymes across all samples precludes any interpretation of whether there has been retargeting of these enzymes associated with loss of mitochondrial tRNA genes.

Mitochondrial ribosomal subunit gene loss, transfer, and replacement in Silene conica

The *S. conica* mitogenome has lost most of the genes that encode ribosomal protein subunits, retaining only three (*rpl5*, *rps3*, and *rps13*) of the 15 that were present in most recent common ancestor of angiosperms (Adams, Qiu, et al. 2002; Kubo and Arimura 2010; Sloan, Alverson, Chuckalovcak, et al. 2012). Although *rps3* was originally annotated as a pseudogene in the *S. conica* mitogenome due to the apparent loss of the first exon and the presence of large indels (Sloan, Alverson, Chuckalovcak, et al. 2012), we detected Rps3 peptides via LC-MS/MS, indicating that it remains an expressed, functional gene. More generally, our proteomic dataset provides insights into how the extensive gene loss from the mitogenome occurred without disrupting function of the mitochondrial ribosome (mitoribosome). Our results point to diverse mechanisms by which these genes were replaced (Figure 5; Table 3).

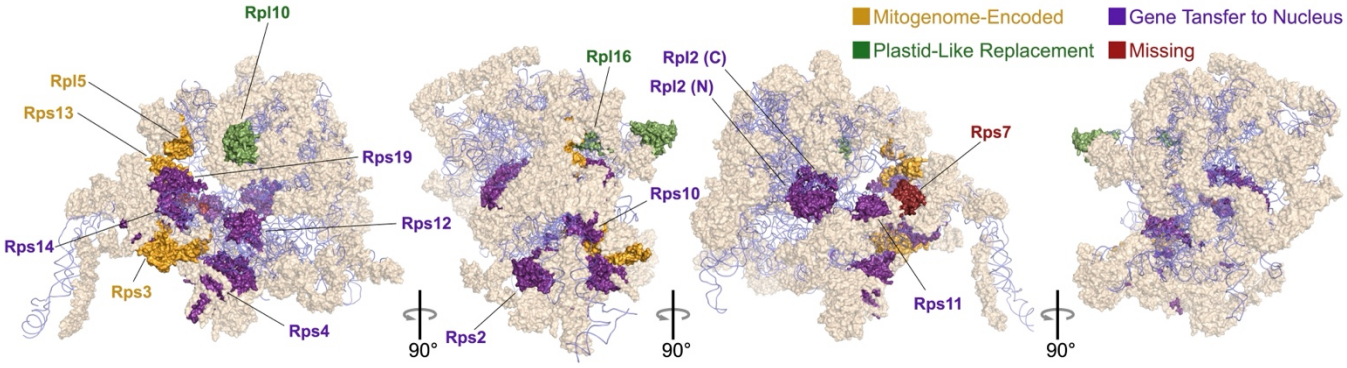

Figure 5. Structure of *A. thaliana* mitoribosome (PDB accession 6XYW; Waltz et al. 2020). Ribosomal proteins are shown with surface renderings, and rRNAs are shown in blue with cartoon renderings. Subunits that were encoded by genes in the ancestral angiosperm mitogenome are highlighted and colored according to their evolutionary history in *S. conica*. Note that the Rps1 subunit is not pictured because it has been lost in *A. thaliana* (Skaltsogiannis et al. 2024) even though the gene is retained in most angiosperms, including the copy that has been transferred to the nucleus in *S. conica* (Table 3).

Nine of the twelve genes that have been lost (*rpl2*, *rps1*, *rps2*, *rps4*, *rps10*, *rps11*, *rps12*, *rps14*, and *rps19*) have followed the typical route of intracellular gene transfer from the mitogenome to the nucleus (Adams and Palmer 2003). In two of these cases (*rpl2* and *rps4*), the transfer appears to have occurred in two pieces, resulting in different nuclear genes encoding separate, non-overlapping portions of each subunit (Table 3).

Two more genes absent from the *S. conica* mitogenome (*rpl10* and *rpl16*) also appear to have been functionally replaced through import of a nuclear-encoded protein. However, in these cases, the nuclear

338 gene is plastid-like rather than an intracellular transfer of the mitochondrial gene itself. The nuclear gene
339 encoding the plastid-targeted Rpl10 subunit in *S. conica* has been duplicated, with one copy now targeted
340 exclusively to the mitochondria based on our LC-MS/MS data. Although many angiosperms retain the *rpl10*
341 gene in the mitogenome, similar duplications and neofunctionalization of plastid-targeted homologs were
342 previously identified in monocots and in the Brassicaceae (Mower and Bonen 2009; Kubo and Arimura
343 2010). In the case of *rpl16*, the *S. conica* nuclear genome contains a plastid-like gene copy encoding a
344 protein that we exclusively detected in the mitochondrial fraction, and the *S. conica* plastid genome still
345 contains a typical *rpl16* gene. As such, it appears that a copy of the plastid *rpl16* gene was transferred to
346 the nucleus but gained targeting to the mitochondria, facilitating the loss of its mitochondrial homolog.
347 This scenario differs from the case of *rpl10* because there is no indication that the transferred *rpl16* gene
348 was ever targeted back to the plastid. Therefore, this evolutionary transition may have required overcoming
349 multiple barriers almost simultaneously. Specifically, the transferred nuclear gene would have had to gain
350 expression and targeting to the mitochondria but also adapt to function in the novel context of the
351 mitoribosome.

352 The one other ribosomal gene that has been lost from the *S. conica* mitogenome (*rps7*) has no
353 detectable homolog in the nuclear genome other than the distantly related family member that encodes a
354 subunit of the cytosolic ribosome (*RPS5*; Sconica_v3_48856-RA). The plastid *rps7* homolog is still retained
355 in the plastid genome itself. Across angiosperm diversity, the *rps7* gene has been subject to an unusually
356 large number of losses from the mitogenome (Adams, Qiu, et al. 2002). Although there are cases where
357 loss of the mitochondrial copy of *rps7* appears to have been accompanied by transfer to the nucleus (Liu et
358 al. 2009), outright loss of the gene may also be common (Adams, Qiu, et al. 2002). The *S. conica* cytosolic-
359 like homolog (Sconica_v3_48856-RA) was detectable in all three sample types. However, proteomic
360 detection in the mitochondrial fraction should not be taken as strong evidence for function within the
361 mitochondria given the extremely high abundance of cytosolic ribosomes and the propensity for these
362 ribosomes to adhere to outer mitochondrial membranes (Chang et al. 2024; Dimnet et al. 2024). Therefore,
363 it is not clear if or how the Rps7 subunit has been replaced in the mitoribosome.

364 Even in angiosperms that have retained a larger number of ribosomal genes in their mitogenomes
365 than *S. conica*, the majority of mitoribosome subunits are encoded by nuclear genes. The composition of
366 the *A. thaliana* mitoribosome has been thoroughly characterized (Rugen et al. 2019; Waltz et al. 2019;
367 Waltz et al. 2020; Skaltsogiannis et al. 2024), so we used proteomic data from the *S. conica* mitochondrial
368 fraction to infer whether these subunits are conserved in the *S. conica* mitoribosome. Of the 70 nuclear-
369 encoded subunits of the *A. thaliana* mitoribosome (Table S2), only bL32m (AT1G26740) lacks a detectable
370 ortholog among the annotated *S. conica* protein set, and this appears to be an annotation issue because
371 homologous sequence is detectable with a TBLASTN search against the *S. conica* nuclear genome. Only

three of the annotated proteins (bS21m, mS38, and bTHXm) were not detected in any of our samples, and every one of the proteins that was detected had higher PSM counts in the mitochondrial fraction than in chloroplast or total leaf samples. Indeed, more than 90% of these proteins were exclusively found in the mitochondrial fraction (Table S2). Therefore, orthologous gene content and mitochondrial proteomes suggest a high degree of stability in the ancestral nuclear-encoded components of the *S. conica* mitoribosome, although confirming that they are assembled as part of the ribosome complex would require purification and structural analysis of the mitoribosomes themselves.

Conclusions

The ongoing loss of angiosperm mitochondrial genes has been well characterized for more than two decades, with especially pronounced effects on the genes encoding translational machinery such as tRNAs and ribosomal proteins (Adams, Qiu, et al. 2002; Richardson et al. 2013). However, direct proteomic analysis of mitochondrial translation machinery has been lacking in species such as *S. conica* that show extreme reductions in mitochondrial gene content. Our study details the extensive changes that accompany mitochondrial gene loss, highlighting alternative evolutionary pathways for functionally replacing genes and responding to perturbations in the network of tRNA-interacting enzymes.

For example, our work confirms that numerous cytosolic-like aaRSs have been retargeted to the mitochondria in *S. conica* (Figure 3), thereby preserving ancestral charging relationships with cytosolic tRNAs that are newly imported into the mitochondria (Warren et al. 2023). We found that this set of retargeted cytosolic-like aaRSs includes SerRS even though *in silico* predictions suggested that it has not gained an N-terminal extension that could serve as a mitochondrially targeting transit peptide (Warren et al. 2023). This finding illustrates why direct proteomic analysis is an important complement to *in silico* predictions and assays based on fusing reporters to N-terminal peptides (Mireau et al. 1996; Uwer et al. 1998; Souciet et al. 1999; Peeters et al. 2000; Duchêne et al. 2001; Duchêne et al. 2005; Warren et al. 2021). On the other hand, our work also shows that many cytosolic-like aaRSs were not retargeted to the mitochondria despite import of their cognate cytosolic tRNAs. Therefore, organellar-like aaRSs are presumably charging novel substrates (cytosolic-like tRNAs) in these cases.

Likewise, functional replacement of mitochondrial ribosomal protein genes appears to have followed multiple pathways (Figure 5), including relocation of the gene to the nucleus, replacement by a plastid-like counterpart, or (in the case of *rps7*) outright loss or replacement with a subunit lacking detectable homology. Overall, the recent evolutionary changes in *S. conica* highlight that the composition

405 of plant mitochondrial translation machinery is still highly dynamic despite billions of years since the
406 establishment of mitochondria in the eukaryotic lineage.
407
408
409 **Materials and Methods**
410
411 *Plant growth and organelle isolations*
412 *Arabidopsis thaliana* Col-0 seeds were stratified at 4 °C in water for 3 days prior to sowing in 3-inch pots
413 with 5 seeds per pot. *Agrostemma githago* KEW0053084 (Warren et al. 2023) and *S. conica* ABR (Fields et
414 al. 2023) were sown in 4-inch pots with 6 seeds per pot. Pots contained Pro-Mix BX potting media and were
415 covered with clear plastic domes for ~1 week until seedlings emerged. All plants were grown on shelves
416 with fluorescent lighting (~100 μE m^{-2} sec^{-1}) at ~22-23 °C under short-day conditions (10-hr light / 14-hr
417 dark). Tissue for total leaf protein samples for all species was harvested at ~12 weeks after sowing.
418 Mitochondrial and chloroplast isolations were performed with tissue harvested either ~9 weeks after
419 germination (*A. thaliana* and *A. githago*) or ~12 to 13 weeks after germination (*S. conica*).
420 Two biological replicates were performed for each species. Mitochondrial and chloroplast
421 fractions were isolated with Percoll gradients. Mitochondrial isolations were performed as described
422 previously (Warren et al. 2021) based on a modified protocol from Meyer et al. (2009), using ~70 g of
423 rosette leaf tissue per replicate. Chloroplast isolations were performed using a modified version of
424 published protocols (van Wijk et al. 2007; Kley et al. 2010). Briefly, ~2 g of rosette leaf tissue was ground in
425 a prechilled mortar with 20 ml of ice-cold chloroplast grinding and wash buffer (cpGW: 50mM HEPES pH
426 7.5, 5 mM EDTA, 0.3 M sorbitol, 10 mM NaHCO3, 0.5 mM DTT), filtered through miracloth and centrifuged
427 at 1,300 rcf for 5 min at 4 °C. The resulting chloroplast pellet was resuspended in ~2 ml cpGW, applied to a
428 Percoll step gradient (40-80%) and centrifuged at 2,500 rcf in a swinging bucket rotor for 10 min at 4 °C. The
429 chloroplast band at the 40-80 interface was removed and washed three times with cpGW buffer.
430 Chloroplasts were resuspended in 1 ml of cpGW buffer containing 1X Halt protease inhibitor (Thermo
431 Scientific 78430), aliquoted and centrifuged at 1,000 rcf for 5 min at 4 °C. Detailed versions of the isolation
432 protocols are available via GitHub (https://github.com/dbsloan/silene_proteomics). Whole leaf tissue and
433 isolated mitochondrial/chloroplast pellets were flash frozen in liquid N_2 and stored at -80 °C before
434 shipment to the Proteome Exploration Laboratory at the California Institute of Technology for protein
435 extraction, digestion, and LC-MS/MS analysis.
436
437 *Protein extraction and digestion*

438 For leaf and purified chloroplast samples, 100 μl of lysis buffer from a PreOmics iST Kit was added and
439 followed by processing with a PreOmics BeatBox Tissue Homogenizer (Preomics, Germany) for 10 min on
440 the high setting. Samples were then centrifuged at 21,000 rcf for 2 min to remove the insoluble fraction.
441 Protein concentration was evaluated using Pierce BCA Protein Assay Kit. Aliquots containing 100 μg of
442 protein from each sample were digested with ProtiFi S-trap according to the manufacturer's protocol.
443 Briefly, the protein was reduced and alkylated with tris(2-carboxyethyl)phosphine and chloroacetamide
444 and digested overnight with trypsin. Following elution, the resulting peptides were dried and resuspended,
445 using 2% acetonitrile, 0.2% formic acid in water.
446 For purified mitochondria samples, which were smaller and contained less protein content, pellets
447 were resuspended in 120 μl of 8 M urea with 50 mM HEPES. Samples were reduced with tris(2-
448 carboxyethyl)phosphine (10 min, 60 °C) and chloroacetamide (15 min, room temperature). Samples were
449 then treated with 2 μl 0.1 mg/ml LysC endopeptidase (Wako Pure Chemical) for 2 hr at 37 °C. Following
450 sample dilution with 360 μl of 50 mM HEPES, 5 μl of 100 mM $CaCl_2$ and 3 μl of the 0.1 mg/ml Trypsin
451 (Pierce) were added for overnight digestion at 37 °C. The digested peptides were desalted using Pierce C18
452 Spin Columns according to the manufacturer's protocol. The eluates were dried and resuspended using
453 2% acetonitrile, 0.2% formic acid in water.
454
455 *LS-MS/MS*
456 For each sample, 500 ng was loaded onto a Thermo Scientific EASY-nLC 1200 connected to an Q Exactive
457 HF Quadrupole-Orbitrap Hybrid Mass Spectrometer. Peptides were separated on an Aurora UHPLC
458 Column (25 cm × 75 μm, 1.6 μm C18, AUR2-25075C18A, Ion Opticks) with a flow rate of 0.35 μl/min for a
459 total duration of 160 min, including washing and re-equilibration. The gradient was composed of 2%
460 Solvent B from the start, 2-6% B for 3.5 min, 6-25% B for 97 min, 25-40% B for 19.5 min, 40-98% B for 2 min,
461 98% B for 3 min, and 98-2% B for 2 min. The gradient was followed by 3 "see-saw" cycles (2% B for 3 min, 2-
462 98% B for 2 min, 98% B for 3 min, and 98-2% B for 2 min) for cleaning, and the column was re-equilibrated
463 at 2% B for 3 min. Solvent A consisted of 97.8% H_2O, 2% acetonitrile, and 0.2% formic acid, and solvent B
464 consisted of 19.8% H2O, 80% acetonitrile, and 0.2% formic acid. Peptides were ionized via electrospray
465 ionization (NSI) at 2.0 kV. MS1 scans were acquired with a range of 350–1600 m/z at 60K resolution. The
466 maximum injection time was 15 ms with an AGC target of 3×10^6. MS2 scans were acquired at 30K
467 resolution with a scan range of 200-2000 m/z. The maximum injection time was 45 ms with a minimum
468 AGC target of 4.5×10^3. The isolation window was 1.2 m/z, collision energy was 28 NCE, and loop count
469 was set to 12. Mass spectrometer method modification and data collection were performed using Thermo
470 Scientific Xcalibur software.

471 Data analysis was performed using Proteome Discoverer 2.5, reference databases from the
472 respective species (see below), and Sequest HT with Percolator validation. Percolator FDRs were set at
473 0.01 (strict) and 0.05 (relaxed). Peptide FDRs were set at 0.01 (strict) and 0.05 (relaxed), with medium
474 confidence and a minimum peptide length of 6. Carbamidomethyl (C) was set as a static modification;
475 oxidation (M) was set as a dynamic modification; acetyl (protein N-term), Met-loss (Protein N-term M), and
476 Met-loss + acetyl (Protein N-term M) were set as dynamic N-Terminal modifications. PSM counts were not
477 reported separately by sample in our initial Proteome Discoverer run, so data were later reanalyzed with
478 Proteome Discover 3.1 to obtain these counts with equivalent settings as above except that Met-loss
479 modifications were not used, and minimum peptide confidence was set to high.
480 Sequence for the *A. thaliana* reference protein database were obtained from the 2023-10 release of
481 PeptideAtlas (van Wijk et al. 2021) and included the Araport11 (Cheng et al. 2017) nuclear-encoded protein
482 sequences (longest isoform only) combined with the mitochondrial-encoded and plastid-encoded
483 proteins curated by van Wijk et al. (2024). Loci in the large insertion of mitochondrial DNA in nuclear
484 chromosome 2 (Stupar et al. 2001; Fields et al. 2022) that are annotated as functional protein-coding
485 genes in the Araport11 database were removed from the reference to avoid ambiguity in mapping to the
486 true mitochondrial-encoded proteins. For *S. conica*, annotated protein sequences were taken from the
487 published nuclear (Fields et al. 2023), mitochondrial (Sloan, Alverson, Chuckalovcak, et al. 2012), and
488 plastid genomes (Sloan, Alverson, Wu, et al. 2012). As with *A. thaliana*, annotated genes found in recent
489 insertions of mitochondrial or plastid DNA into the nucleus were removed from the reference. We also
490 added three aaRS protein sequences that were previously identified with full-length RNA-seq transcripts
491 (Warren et al. 2023) but were not annotated in the published *S. conica* genome (Iso-Seq AspRS, HisRS, and
492 ValRS). Mitochondrial-encoded and plastid-encoded protein sequences for *A. githago* were taken from
493 published genomes (Sloan et al. 2014; Warren et al. 2021). Because no reference-quality annotation was
494 available for the *A. githago* nuclear genome (although one has since been published; Mian and Leitch
495 2024), we used previously published full-length RNA-seq transcripts (Warren et al. 2023) for nuclear-
496 encoded protein references. The longest open-reading frame for each transcript was identified with
497 TransDecoder v5.7.1, and the corresponding protein-coding sequences with >99% identity were collapsed
498 with CD-HIT v4.8.1 (Fu et al. 2012). This transcriptome reference for *A. githago* was then filtered to avoid
499 duplicating annotated proteins from the mitochondrial and plastid reference genomes.
500
501 *Enrichment analysis of mitochondrial-encoded and plastid-encoded proteins*
502 For each species, enrichment of mitochondrial-encoded and plastid-encoded proteins in the organellar
503 fractions was calculated as the PSM count ratio in the corresponding organellar sample relative to total
504 leaf tissue. PSM counts for the two biological replicates from each sample type were summed for these

505 calculations. Proteins with fewer than 5 PSMs in total across all samples from a species were excluded. In
506 cases where no PSMs were detected in the leaf tissue (but were detected in an organellar fraction), a
507 minimum count of 1 was applied for the leaf sample to avoid dividing by 0. Enrichment ratios were also
508 calculated based on ion intensity by using the reported abundance values from Proteome Discoverer. For
509 these calculations, proteins were only considered to be detected in a sample if they were assigned "high"
510 confidence based on identification of a corresponding PSM in that sample. Proteins that were only
511 identified in a sample based on comparisons of peak positions to other samples with detected PSMs were
512 treated as not found. Low or missing abundance values were set to a minimum floor value (0.1 percentile
513 in the corresponding sample), and all values were normalized to the median abundance in the sample.
514
515 *Analysis of aaRSs and other tRNA metabolism enzymes*
516 To investigate the subcellular localization of previously identified aaRSs (Duchêne et al. 2005; Duchêne et
517 al. 2009; Warren et al. 2023), PSM enrichment ratios were calculated as described above for the
518 organellar-encoded proteins. To assess how relative aaRS abundance within the mitochondria differed
519 between species, we calculated a metric of enrichment bias between organellar-like and cytosolic-like
520 counterparts. Specifically, the mitochondrial enrichment ratio (see above) for the cytosolic-like aaRS was
521 divided by the sum of the mitochondrial enrichment ratios for the organellar-like and cytosolic-like aaRSs.
522 Therefore, a value of 1 for this metric would indicate that only the cytosolic-like aaRS was found in the
523 mitochondria, whereas a values of 0 would indicate that only the organellar-like aaRS was found. When
524 both types were detected in the mitochondria, this metric produces an intermediate value that reflects the
525 relative bias of organellar-like vs. cytosolic-like types. By using the enrichment ratios in these calculations,
526 we were able to normalize to the total leaf samples and avoid directly comparing raw PSM counts between
527 different proteins. We summed PSM counts in cases where there were multiple proteins or subunits for the
528 same aaRS class. For some proteins, we found very low PSM counts in leaf tissue, resulting in large and
529 highly variable enrichment ratios. Therefore, we capped enrichment ratios at a value of 3 to avoid
530 obscuring signal of co-existing aaRS types based on these inflated values.
531 PheRS and tRNA-Phe sequences were obtained via SHOOT (Emms and Kelly 2022), BLASTP
532 searches of the NCBI RefSeq database (Pruitt et al. 2004), and previously curated datasets (Warren et al.
533 2021; Warren et al. 2023; DeTar et al. 2024). Alignments were performed with MAFFT v7.526 (Katoh and
534 Standley 2013) under default parameters and visualized with Geneious (Kearse et al. 2012). The structure
535 of the *S. conica* PheRS/tRNA-Phe complex was predicted using the AlphaFold3 Server (Abramson et al.
536 2024) under default parameters. The mitochondrial PheRS and cytosolic tRNA-Phe sequences were
537 obtained from previous studies (Warren et al. 2021; Warren et al. 2023). The first 49 amino acids were
538 removed from the PheRS sequence as a putative transit peptide.

539 The *A. thaliana* genes encoding GatCAB, MTF, TilS, PRORP, tRNase Z, and CCAse proteins were
540 previously identified (von Braun et al. 2007; Pujol et al. 2008; Canino et al. 2009; Gutmann et al. 2012;
541 Warren and Sloan 2020). We used reciprocal BLASTP searches against the annotated proteins sequences
542 from the *S. conica* genome to identify orthologs and inferred presence of the enzymes in organellar
543 fractions based on PSM counts as described above.
544
545 *Analysis of mitoribosome subunits*
546 The set of *A. thaliana* mitoribosome subunits was taken from the published structure (Waltz et al. 2020).
547 We also included the uL1m (AT2G42710) and bL12m (AT3G06040) subunits, which were not captured in
548 this structure presumably because they are located in highly mobile parts of the ribosome (Waltz et al.
549 2020). We used the mitochondrial-encoded Rps1 subunit from *Carica papaya* because this protein is
550 known to have been lost entirely from *A. thaliana* (Skaltsogiannis et al. 2024). Reciprocal BLASTP searches
551 were used to identify *S. conica* orthologs, and we inferred presence of subunits in the mitochondrial
552 fraction based on PSM data as described above. Some ribosomal subunits were encoded by two or more
553 closely related paralogs, and some reciprocal BLASTP searches failed due to this paralogy. In other cases,
554 no PSMs were detected in any sample for the named subunit in the *A. thaliana* mitoribosome structure. In
555 these cases, closely related paralogs were manually checked and substituted in where necessary. The
556 mitoribosome structure was visualized with PyMol v3.1.3, using Protein Data Bank accession 6XYW (Waltz
557 et al. 2020).
558
559
560 **Data Availability**
561 LC-MS/MS data have been deposited to the ProteomeXchange Consortium via the PRIDE (Pérez-Riverol et
562 al. 2024) partner repository with the dataset identifier PXD071069. Code and processed data are available
563 via GitHub (https://github.com/dbsloan/silene_proteomics).
564
565
566 **Acknowledgements**
567 We thank Baiyi Quan and the Proteome Exploration Laboratory at the California Institute of Technology for
568 performing LC-MS/MS runs and data processing. This work was supported by a grant from the National
569 Science Foundation (MCB-2048407) and an HHMI Hanna H. Gray Fellowship.

Table 1. Detected proteins in LC-MS/MS dataset

	Detected Proteins[a]	
Sample Type	***Arabidopsis***	***Silene***
Mitochondria	2832	2494
Chloroplasts	2118	1974
Leaf Tissue	4371	4294
Total (any sample)	5599	5491

[a] Proteins were only included in counts if a corresponding PSM was identified in either or both replicates for that sample type. Identifications based solely on a peak position that matches a PSM from another sample type were not included.

Table 2. Comparison between aaRS detection in LC-MS/MS dataset and previous classification of subcellular localization (Duchêne et al. 2005; Duchêne et al. 2009)

Accession	Type	Duchêne Classification	Potential Refinements	Notes
AT5G22800	AlaRS	Chloro-Mito	Chloro-only	No mito localization detected
AT1G50200	AlaRS	Cyto-Chloro-Mito	Cyto-Mito	No chloroplast localization detected
AT4G26300	ArgRS	Cyto-Chloro-Mito(?)	Cyto-Chloro-Mito	Mito localization confirmed
AT1G66530	ArgRS	Cyto-only(?)	No change	
AT4G17300	AsnRS	Chloro-Mito	No change	
AT5G56680	AsnRS	Cyto-only	No change	
AT1G70980[a]	AsnRS	Cyto-only	No change	
AT4G33760	AspRS	Chloro-Mito	No change	
AT4G31180	AspRS	Cyto-only	No change	
AT4G26870	AspRS	Cyto-only	No change	
AT2G31170	CysRS	Chloro-Mito	No change	
AT5G38830	CysRS	Cyto-only	No change	
AT3G56300[a]	CysRS	Cyto-only	No change	
AT1G25350	GlnRS	Cyto-only	No change	
AT5G64050	GluRS	Chloro-Mito	No change	
AT5G26710	GluRS	Cyto-only	No change	
AT3G48110	GlyRS	Chloro-Mito	No change	
AT1G29880	GlyRS	Cyto-Mito*	No change	
AT3G46100	HisRS	Chloro-Mito	No change	
AT3G02760	HisRS	Cyto-only	No change	
AT5G49030	IleRS	Chloro-Mito	No change	
AT4G10320	IleRS	Cyto-only	No change	
AT4G04350	LeuRS	Chloro-only	No change	
AT1G09620	LeuRS	Cyto-Mito	No change	
AT3G13490	LysRS	Chloro-Mito	No change	
AT3G11710	LysRS	Cyto-only	No change	
AT3G55400	MetRS	Chloro-Mito	No change	
AT4G13780	MetRS	Cyto-only	No change	
AT3G58140	PheRS	Chloro-Mito	No change	
AT4G39280	PheRS	Cyto-only	No change	
AT1G72550	PheRS	Cyto-only	No change	
AT5G52520	ProRS	Chloro-Mito	No change	
AT3G62120	ProRS	Cyto-only	No change	
AT1G11870	SerRS	Chloro-Mito	No change	
AT5G27470	SerRS	Cyto-only	No change	
AT2G04842	ThrRS	Chloro-Mito	Chloro-only	No mito localization detected
AT5G26830	ThrRS	Cyto-Mito	No change	
AT1G17960[a]	ThrRS	Cyto-only	No change	
AT2G25840	TrpRS	Chloro-Mito	No change	
AT3G04600	TrpRS	Cyto-only	No change	
AT3G02660	TyrRS	Chloro-Mito	No change	
AT1G28350	TyrRS	Cyto-only	No change	
AT2G33840[a]	TyrRS	Cyto-only	No change	
AT5G16715	ValRS	Chloro-Mito	Chloro-only(?)	Only weak mito localization detected
AT1G14610	ValRS	Cyto-Mito*	Cyto-Mito(?)	May be functional in mito given low detection of AT5G16715 in mito

[a] Four aaRSs were not detected in our proteomic dataset (all predicted to be cyto-only and close paralogs of aaRSs that were detected).

Table 3. Genes encoding subunits of the mitoribosome that were ancestrally present in the angiosperm mitogenone

			***Silene* PSM Counts**					
Protein	***Silene* gene ID**[a]	***Arabidopsis* gene ID**[a]	**Mt1**	**Mt2**	**Cp1**	**Cp2**	**Leaf1**	**Leaf2**
Rpl2 N-term (uL2m)	Chr03-anno2.g23183.t1	***mito rpl2***	6	7	0	0	0	0
Rpl2 C-term (uL2m)	Sconica_v3_41290-RA	AT2G44065	9	11	0	0	0	0
Rpl5 (uL5m)	***mito rpl5***	***mito rpl5***	6	2	0	0	0	0
Rpl10 (uL10m)	Sconica_v3_43288-RA[b]	AT3G12370[b]	6	3	0	0	0	0
Rpl16 (uL16m)	Sconica_v3_30744-RA[b]	***mito rpl16***	8	3	0	0	0	0
Rps1 (uS1)	Sconica_v3_17748-RA	Lost in *A. thaliana*	9	6	0	0	0	0
Rps2 (uS2m)	Sconica_v3_17930-RA	AT3G03600	13	7	0	0	0	0
Rps3 (uS3m)	***mito rps3***	***mito rps3***	24	17	0	0	0	0
Rps4 N-term (uS4m)	FUN_045851-T1/FUN_045790-T1	***mito rps4***	5	7	0	0	0	0
Rps4 C-term (uS4m)	Sconica_v3_40630-RA	***mito rps4***	10	3	0	0	0	0
Rps7 (uS7m)	Lost in *S. conica*	***mito rps7***	NA	NA	NA	NA	NA	NA
Rps10 (uS10m)	Sconica_v3_23770-RA	AT3G22300	7	5	0	0	0	0
Rps11 (uS11m)	Sconica_v3_11125-RA	AT1G31817	8	2	0	0	0	0
Rps12 (uS12m)	Sconica_v3_11465-RA	***mito rps12***	5	2	0	0	0	0
Rps13 (uS13m)	***mito rps13***	AT1G77750[b]	3	5	0	0	0	0
Rps14 (uS14m)	FUN_029269-T1	AT2G34520	2	5	0	0	0	0
Rps19 (uS19m)	Sconica_v3_16857-RA	AT5G47320	1	2	0	0	0	0

[a]Names in bold italics correspond to genes in the mitogenome. All others are in the nuclear genome.

[b]The genes encoding Rps13 in *Arabidopsis*, Rpl16 in *Silene*, and Rpl10 in both species are duplications of their plastid counterparts and not derived from the ancestral mitochondrial gene (Adams, Daley, et al. 2002; Mower and Bonen 2009; Kubo and Arimura 2010).

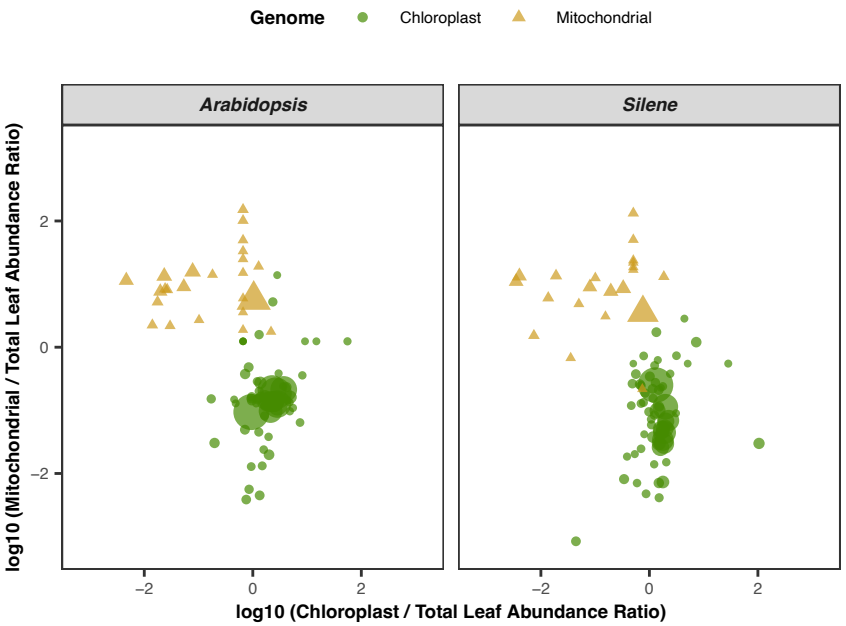

Figure S1. Enrichment of proteins encoded by the organellar genomes in purified chloroplast fractions (x-axis) and mitochondrial fractions (y-axis). Enrichment ratios are quantified based on summed abundance values (peak areas) from two replicates relative to abundances in leaf tissue samples. Each point represents a protein, and point sizes are scaled proportionally to the total number of PSMs observed for the corresponding protein across all samples. Plastid-encoded proteins and mitochondrial-encoded proteins and are represented by green circles and gold triangles, respectively.

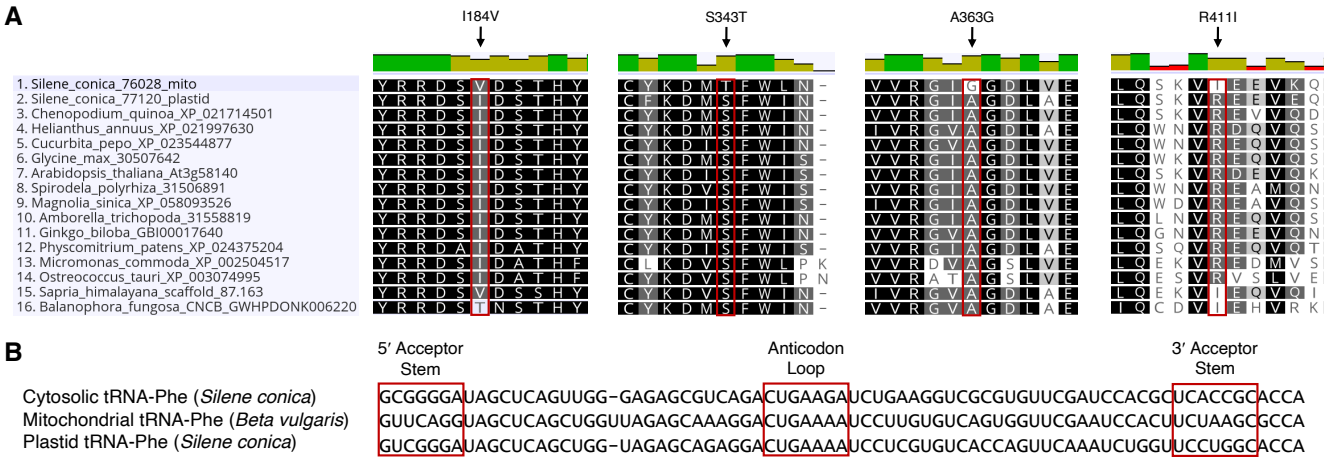

Figure S2. PheRS and tRNA-Phe alignments. (A) Amino acid alignments showing four positions in the PheRS sequence that have a derived change in the *Silene conica* mitochondrial PheRS but are otherwise conserved across a diverse sampling of green plants/algae. In two of these cases (I184V and R411I), parallel substitutions are observed in the parasitic plant taxa *Sapria himalayana* and *Balanophora fungosa*. (B) Alignment of cytosolic, mitochondrial, and plastid tRNA-Phe.

Table S1. PSM counts by sample for additional enzymes involved in tRNA metabolism in mitochondria and other compartments

	Arabidopsis thaliana							*Silene conica*						
Enzyme	**AGI ID**	**Mt1**	**Mt2**	**Cp1**	**Cp2**	**Leaf1**	**Leaf2**	**Gene ID**	**Mt1**	**Mt2**	**Cp1**	**Cp2**	**Leaf1**	**Leaf2**
GatA	AT3G25660	6	7	7	2	6	3	Sconica_v3_10523-RA	0	0	6	10	3	2
GatB	AT1G48520	8	7	12	3	7	5	Sconica_v3_48968-RA	0	0	12	15	5	1
GatC	AT4G32915	4	3	2	1	0	0	Sconica_v3_42040-RA	0	0	0	5	0	0
CCAse	AT1G22660	0	0	0	0	0	0	FUN_019134-T1	3	2	0	1	1	0
MTF	AT1G66520	1	0	0	0	0	0	Sconica_v3_07812-RA	7	4	7	10	6	2
TilS	AT3G24560	0	0	0	0	0	0	Chr10-anno1.g29341.t1	1	0	0	0	0	0
tRNase Z1[a]	AT1G74700	0	0	0	0	0	0	FUN_038515-T1	2	0	0	0	0	0
tRNase Z2	AT2G04530	0	0	0	0	0	0	Chr03-anno1.g57321.t1	0	0	1	3	0	0
tRNase Z3	AT1G52160	0	0	0	0	0	0	Multiple	0	0	0	0	0	0
tRNase Z4	AT3G16260	0	0	0	0	0	0	Multiple	0	0	0	0	0	0
PRORP1	AT2G32230	0	0	1	0	0	0	FUN_011644-T1	0	0	2	1	0	0
PRORP2	AT2G16650	0	0	0	0	0	0	No gene found	NA	NA	NA	NA	NA	NA
PRORP3	AT4G21900	0	0	0	0	0	0	No gene found	NA	NA	NA	NA	NA	NA

[a]A second *S. conica* gene had a top BLAST hit to *A. thaliana* tRNase Z1, but no PSMs were detected for it.

Table S2. Genes encoding subunits of the *A. thaliana* mitoribosome (Waltz et al. 2020) and their counterparts in *S. conica*

			***Silene* PSM Counts**					
Protein	***Silene* gene ID[a]**	***Arabidopsis* gene ID[a]**	**Mt1**	**Mt2**	**Cp1**	**Cp2**	**Leaf1**	**Leaf2**
uL1m	Sconica_v3_19193-RA	AT2G42710	15	11	1	0	0	0
uL2m N-term	Chr03-anno2.g23183.t1	***mito rpl2***	6	7	0	0	0	0
uL2m C-term	Sconica_v3_41290-RA	AT2G44065	9	11	0	0	0	0
uL3m	Sconica_v3_37834-RA	AT3G17465	8	8	0	0	0	0
uL4m	Sconica_v3_19156-RA	AT2G20060	8	5	0	0	0	1
uL5m	***mito rpl5***	***mito rpl5***	6	2	0	0	0	0
uL6m	Chr08-anno2.g6040.t1	AT2G18400	0	3	0	0	0	0
bL9m	FUN_038434-T1	AT5G53070	5	5	0	0	0	0
uL10m	Sconica_v3_43288-RA	AT3G12370	6	3	0	0	0	0
uL11m	Chr03-anno1.g57427.t1	AT4G35490	7	3	0	0	0	0
bL12m	Sconica_v3_40269-RA	AT3G06040	11	12	0	0	0	0
uL13m	Chr04-anno1.g50273.t1	AT3G01790	8	5	0	0	0	0
uL14m	FUN_046256-T1	AT5G46160	5	4	0	0	0	0
uL15m	Sconica_v3_17785-RA	AT5G64670	9	7	0	0	0	0
uL16m	Sconica_v3_30744-RA	***mito rpl16***	8	3	0	0	0	0
bL17m	Sconica_v3_10014-RA	AT5G09770	3	3	0	0	0	0
uL18m	Sconica_v3_57073-RA	AT5G27820	7	5	0	0	0	0
bL19m	FUN_019669-T1	AT1G24240	6	7	0	0	0	0
bL20m	Sconica_v3_23041-RA	AT1G16740	6	5	0	0	0	0
bL21m	Sconica_v3_47180-RA	AT4G30930	8	6	0	0	0	0
uL22m	Sconica_v3_06702-RA	AT1G52370	9	7	0	0	0	0
uL23m	Chr08-anno1.g34018.t1	AT4G39880	8	6	0	0	0	0
uL24m	Sconica_v3_17854-RA	AT5G23535	3	5	0	0	0	0
bL25m	Sconica_v3_43645-RA	AT5G66860	7	8	0	0	0	0
bL27m	Sconica_v3_22742-RA	AT2G16930	3	2	0	0	0	0
bL28m	Chr10-anno1.g32626.t1	AT4G31460	11	8	0	0	0	0
uL29m	Sconica_v3_24808-RA	AT1G07830	4	1	0	0	0	0
uL30m	Sconica_v3_42097-RA	AT5G55140	3	1	0	0	0	0
bL31m	Chr03-anno2.g23587.t1	AT5G55125	2	1	0	0	0	0
bL32m	Not annotated	AT1G26740	N/A	N/A	N/A	N/A	N/A	N/A
bL33m	Sconica_v3_46773-RA	AT5G18790	2	0	0	0	1	0
bL35m	Chr02-anno1.g23806.t1	AT5G45590	3	2	0	0	0	0
bL36m	Chr09-anno2.g40880.t1	AT5G20180	1	0	0	0	0	0
mL40	Chr04-anno1.g46970.t1	AT4G05400	3	3	0	1	0	0
mL41	FUN_023568-T1	AT5G40080	1	3	0	0	0	0
mL43	Chr10-anno1.g28670.t1	AT3G59650	4	2	0	0	0	0
mL46	Sconica_v3_41121-RA	AT1G14620	13	9	0	0	1	0
mL53	Sconica_v3_53235-RA	AT5G39600	8	3	0	0	0	0
mL59/mL64	Chr06-anno1.g19483.t1	AT4G22000	6	1	0	0	0	0
mL60	Sconica_v3_30462-RA	AT1G27435	1	3	0	0	0	0
mL80	Chr01-anno1.g62765.t1	AT1G73940	6	1	0	0	0	0
mL87	Sconica_v3_10159-RA	AT3G51010	3	2	0	0	0	0
mL101 (rPPR4)	Sconica_v3_25967-RA	AT1G60770	9	7	0	0	0	0
mL102 (rPPR5)	Sconica_v3_09229-RA	AT2G37230	27	23	0	0	0	0
mL104 (rPPR9)	Sconica_v3_02474-RA	AT5G60960	19	17	0	0	0	0
uS1	Sconica_v3_17748-RA	Lost in *Arabidopsis*	9	6	0	0	0	0
uS2m	Sconica_v3_17930-RA	AT3G03600	13	7	0	0	0	0
uS3m	***mito rps3***	***mito rps3***	24	17	0	0	0	0

uS4m N-term	FUN_045851-T1/FUN_045790-T1	***mito rps4***	5	7	0	0	0	0
uS4m C-term	Sconica_v3_40630-RA	***mito rps4***	10	3	0	0	0	0
uS5m	Sconica_v3_25633-RA	AT1G64880	18	20	0	0	0	0
bS6m	Sconica_v3_05402-RA	AT3G18760	3	2	0	0	0	0
uS7m	Lost in *Silene*	***mito rps7***	N/A	N/A	N/A	N/A	N/A	N/A
uS8m	Sconica_v3_37372-RA	AT4G29430	3	4	0	0	0	0
uS9m	Sconica_v3_19137-RA	AT3G49080	10	5	0	0	0	0
uS10m	Sconica_v3_23770-RA	AT3G22300	7	5	0	0	0	0
uS11m	Sconica_v3_11125-RA	AT1G31817	8	2	0	0	0	0
uS12m	Sconica_v3_11465-RA	***mito rps12***	5	2	0	0	0	0
uS13m	***mito rps13***	AT1G77750	3	5	0	0	0	0
uS14m	FUN_029269-T1	AT2G34520	2	5	0	0	0	0
uS15m	Sconica_v3_25605-RA	AT1G15810	19	14	0	0	0	0
bS16m	Sconica_v3_11133-RA	AT5G56940	10	5	0	0	0	0
uS17m	Sconica_v3_53755-RA	AT1G49400	11	8	0	0	0	0
bS18m	Chr02-anno1.g21175.t1	AT1G07210	10	9	0	0	0	0
uS19m	FUN_042562-T1	AT5G47320	9	6	0	0	0	0
bS21m	FUN_011913-T1	AT3G26360	0	0	0	0	0	0
mS23	Sconica_v3_11989-RA	AT1G26750	16	12	0	0	0	0
mS26	Sconica_v3_22695-RA	AT5G49210	4	6	0	0	0	0
mS29	Chr04-long_reads1.PB.1859.1	AT1G16870	19	14	0	0	0	0
mS33	Sconica_v3_48073-RA	AT5G44710	4	3	0	0	0	0
mS34	Chr02-anno1.g21262.t1	AT5G52370	7	8	0	0	0	0
mS35	Sconica_v3_02574-RA	AT3G18240	12	7	0	0	0	0
mS37	FUN_006674-T1	AT1G47278	5	4	0	0	0	0
mS38	Sconica_v3_12210-RA	AT5G63150	0	0	0	0	0	0
mS41	Sconica_v3_30872-RA	AT5G26800	2	1	0	0	0	0
mS45	Chr09-anno1.g45083.t1	AT5G62270	7	8	0	0	0	0
mS47	Chr08-anno1.g33382.t1	AT4G31810	15	7	0	0	0	0
mS80 (rPPR6)	Chr10-anno1.g29827.t1	AT3G02650	21	13	0	0	0	0
mS83 (rPPR10)	Sconica_v3_49004-RA	AT4G15640	6	6	0	0	0	0
bTHXm	Chr01-anno1.g64414.t1	AT2G21290	0	0	0	0	0	0

[a]Names in bold italics correspond to genes in the mitogenome. All others are in the nuclear genome.

References

Abramson J, Adler J, Dunger J, Evans R, Green T, Pritzel A, Ronneberger O, Willmore L, Ballard AJ, Bambrick J, et al. 2024. Accurate structure prediction of biomolecular interactions with AlphaFold 3. *Nature* 630:493–500.

Adams KL, Daley DO, Whelan J, Palmer JD. 2002. Genes for two mitochondrial ribosomal proteins in flowering plants are derived from their chloroplast or cytosolic counterparts. *Plant Cell* 14:931–943.

Adams KL, Palmer JD. 2003. Evolution of mitochondrial gene content: gene loss and transfer to the nucleus. *Mol. Phylogenet. Evol.* 29:380–395.

Adams KL, Qiu YL, Stoutemyer M, Palmer JD. 2002. Punctuated evolution of mitochondrial gene content: high and variable rates of mitochondrial gene loss and transfer to the nucleus during angiosperm evolution. *Proc. Natl. Acad. Sci. U. S. A.* 99:9905–9912.

Adams KL, Song K, Roessler PG, Nugent JM, Doyle JL, Doyle JJ, Palmer JD. 1999. Intracellular gene transfer in action: dual transcription and multiple silencings of nuclear and mitochondrial *cox2* genes in legumes. *Proceedings of the National Academy of Sciences* 96:13863–13868.

Berg M, Rogers R, Muralla R, Meinke D. 2005. Requirement of aminoacyl-tRNA synthetases for gametogenesis and embryo development in Arabidopsis: Aminoacyl-tRNA synthetase knockouts. *Plant J.* 44:866–878.

Berrissou C, Cognat V, Koechler S, Bergdoll M, Duchêne A-M, Drouard L. 2024. Extensive import of nucleus-encoded tRNAs into chloroplasts of the photosynthetic lycophyte, Selaginella kraussiana. *Proc. Natl. Acad. Sci. U. S. A.* 121:e2412221121.

Boore JL. 1999. Animal mitochondrial genomes. *Nucleic Acids Res.* 27:1767–1780.

von Braun SS, Sabetti A, Hanic-Joyce PJ, Gu J, Schleiff E, Joyce PBM. 2007. Dual targeting of the tRNA nucleotidyltransferase in plants: not just the signal. *J. Exp. Bot.* 58:4083–4093.

Broz AK, Waneka G, Wu Z, Sloan DB. 2021. Detecting de novo mitochondrial mutations in angiosperms with highly divergent evolutionary rates. *Genetics* 218:iyab039.

Canino G, Bocian E, Barbezier N, Echeverría M, Forner J, Binder S, Marchfelder A. 2009. Arabidopsis encodes four tRNase Z enzymes. *Plant Physiol.* 150:1494–1502.

Ceriotti LF, Roulet ME, Sanchez-Puerta MV. 2021. Plastomes in the holoparasitic family Balanophoraceae: Extremely high AT content, severe gene content reduction, and two independent genetic code changes. *Mol. Phylogenet. Evol.* 162:107208.

Chang Y-T, Barad BA, Rahmani H, Zid BM, Grotjahn DA. 2024. Cytoplasmic ribosomes on mitochondria alter the local membrane environment for protein import. *bioRxivorg* [Internet]. Available from: http://biorxiv.org/lookup/doi/10.1101/2024.07.17.604013

Cheng C-Y, Krishnakumar V, Chan AP, Thibaud-Nissen F, Schobel S, Town CD. 2017. Araport11: a complete reannotation of the Arabidopsis thaliana reference genome. *Plant J.* 89:789–804.

DeTar RA, Chustecki JM, Martinez-Hottovy A, Ceriotti LF, Broz AK, Lou X, Sanchez-Puerta MV, Elowsky C, Christensen AC, Sloan DB. 2024. Photosynthetic demands on translational machinery drive retention of redundant tRNA metabolism in plant organelles. *Proc. Natl. Acad. Sci. U. S. A.* 121:e2421485121.

Dimnet L, Salinas-Giegé T, Pullara S, Moyet L, Genevey C, Kuntz M, Duchêne A-M, Rolland N. 2024. Isolation of cytosolic ribosomes associated with plant mitochondria and chloroplasts. *Methods Mol. Biol.* 2776:289–302.

Duchêne A-M, Giritch A, Hoffmann B, Cognat V, Lancelin D, Peeters NM, Zaepfel M, Maréchal-Drouard L, Small ID. 2005. Dual targeting is the rule for organellar aminoacyl-tRNA synthetases in *Arabidopsis thaliana*. *Proceedings of the National Academy of Sciences* 102:16484–16489.

Duchêne AM, Peeters N, Dietrich A, Cosset A, Small ID, Wintz H. 2001. Overlapping destinations for two dual targeted glycyl-tRNA synthetases in Arabidopsis thaliana and Phaseolus vulgaris. *J. Biol. Chem.* 276:15275–15283.

Duchêne A-M, Pujol C, Maréchal-Drouard L. 2009. Import of tRNAs and aminoacyl-tRNA synthetases into mitochondria. *Curr. Genet.* 55:1–18.

Emms DM, Kelly S. 2022. SHOOT: phylogenetic gene search and ortholog inference. *Genome Biol.* 23:85.

Fields P, Weber MM, Waneka G, Broz A, Sloan DB. 2023. Chromosome-level genome assembly for the angiosperm Silene conica. *Genome Biol. Evol.* 15:evad192.

Fields PD, Waneka G, Naish M, Schatz MC, Henderson IR, Sloan DB. 2022. Complete Sequence of a 641-kb Insertion of Mitochondrial DNA in the Arabidopsis thaliana Nuclear Genome. *Genome Biol. Evol.* 14:evac059.

Fu L, Niu B, Zhu Z, Wu S, Li W. 2012. CD-HIT: accelerated for clustering the next-generation sequencing data. *Bioinformatics* 28:3150–3152.

Gamper H, Hou Y-M. 2020. A label-free assay for aminoacylation of tRNA. *Genes* 11:1173.

Gobert A, Gutmann B, Taschner A, Gössringer M, Holzmann J, Hartmann RK, Rossmanith W, Giegé P. 2010. A single Arabidopsis organellar protein has RNase P activity. *Nat. Struct. Mol. Biol.* 17:740–744.

Gould SB, Waller RF, McFadden GI. 2008. Plastid evolution. *Annu. Rev. Plant Biol.* 59:491–517.

Gutmann B, Gobert A, Giegé P. 2012. PRORP proteins support RNase P activity in both organelles and the nucleus in Arabidopsis. *Genes Dev.* 26:1022–1027.

Ibba M, Söll D. 2004. Aminoacyl-tRNAs: setting the limits of the genetic code. *Genes Dev.* 18:731–738.

Katoh K, Standley DM. 2013. MAFFT multiple sequence alignment software version 7: improvements in performance and usability. *Mol. Biol. Evol.* 30:772–780.

Kearse M, Moir R, Wilson A, Stones-Havas S, Cheung M, Sturrock S, Buxton S, Cooper A, Markowitz S, Duran C. 2012. Geneious Basic: an integrated and extendable desktop software platform for the organization and analysis of sequence data. *Bioinformatics* 28:1647–1649.

Kley J, Heil M, Muck A, Svatos A, Boland W. 2010. Isolating intact chloroplasts from small Arabidopsis samples for proteomic studies. *Anal. Biochem.* 398:198–202.

Klipcan L, Moor N, Finarov I, Kessler N, Sukhanova M, Safro MG. 2012. Crystal structure of human mitochondrial PheRS complexed with tRNAPhe in the active “open” state. *J. Mol. Biol.* 415:527–537.

Kubo N, Arimura S. 2010. Discovery of the rpl10 gene in diverse plant mitochondrial genomes and its probable replacement by the nuclear gene for chloroplast RPL10 in two lineages of angiosperms. *DNA Res.* 17:1–9.

Liu SL, Zhuang Y, Zhang P, Adams KL. 2009. Comparative analysis of structural diversity and sequence evolution in plant mitochondrial genes transferred to the nucleus. *Mol. Biol. Evol.* 26:875–891.

McCutcheon JP, Garber AI, Spencer N, Warren JM. 2024. How do bacterial endosymbionts work with so few genes? *PLoS Biol.* 22:e3002577.

McCutcheon JP, Moran NA. 2012. Extreme genome reduction in symbiotic bacteria. *Nat. Rev. Microbiol.* 10:13–26.

Meiklejohn CD, Holmbeck MA, Siddiq MA, Abt DN, Rand DM, Montooth KL. 2013. An Incompatibility between a mitochondrial tRNA and its nuclear-encoded tRNA synthetase compromises development and fitness in Drosophila. *PLoS Genet.* 9:e1003238.

Meyer EH, Tomaz T, Carroll AJ, Estavillo G, Delannoy E, Tanz SK, Small ID, Pogson BJ, Millar AH. 2009. Remodeled respiration in ndufs4 with low phosphorylation efficiency suppresses Arabidopsis germination and growth and alters control of metabolism at night. *Plant Physiol.* 151:603–619.

Mian S, Leitch IJ. 2024. The genome sequence of the corn cockle, Agrostemma githago L., 1753 (Caryophyllaceae). *Wellcome Open Res.* 9:590.

Mireau H, Lancelin D, Small ID. 1996. The same Arabidopsis gene encodes both cytosolic and mitochondrial alanyl-tRNA synthetases. *Plant Cell* 8:1027–1039.

Molina J, Hazzouri KM, Nickrent D, Geisler M, Meyer RS, Pentony MM, Flowers JM, Pelser P, Barcelona J, Inovejas SA. 2014. Possible loss of the chloroplast genome in the parasitic flowering plant *Rafflesia lagascae* (Rafflesiaceae). *Mol. Biol. Evol.* 31:793–803.

Mower JP, Bonen L. 2009. Ribosomal protein L10 is encoded in the mitochondrial genome of many land plants and green algae. *BMC Evol. Biol.* 9:265.

Peeters NM, Chapron A, Giritch A, Grandjean O, Lancelin D, Lhomme T, Vivrel A, Small I. 2000. Duplication and quadruplication of Arabidopsis thaliana cysteinyl- and asparaginyl-tRNA synthetase genes of organellar origin. *J. Mol. Evol.* 50:413–423.

Pérez-Riverol Y, Bandla C, Kundu DJ, Kamatchinathan S, Bai J, Hewapathirana S, John NS, Prakash A, Walzer M, Wang S, et al. 2024. The PRIDE database at 20 years: 2025 update. *Nucleic Acids Res.* 53:D543–D553.

Pett W, Lavrov DV. 2015. Cytonuclear interactions in the evolution of animal mitochondrial tRNA metabolism. *Genome Biol. Evol.* 7:2089–2101.

Pruitt K, Tatusova T, Maglott D. 2004. NCBI Reference Sequence (RefSeq): a curated non-redundant sequence database of genomes, transcripts and proteins. *Nucleic Acids Research* 33:D501–D504.

Pujol C, Bailly M, Kern D, Marechal-Drouard L, Becker H, Duchene AM. 2008. Dual-targeted tRNA-dependent amidotransferase ensures both mitochondrial and chloroplastic Gln-tRNAGln synthesis in plants. *Proceedings of the National Academy of Sciences* 105:6481–6485.

Richardson AO, Rice DW, Young GJ, Alverson AJ, Palmer JD. 2013. The "fossilized" mitochondrial genome of Liriodendron tulipifera: ancestral gene content and order, ancestral editing sites, and extraordinarily low mutation rate. *BMC Biol.* 11:29.

Roger AJ, Muñoz-Gómez SA, Kamikawa R. 2017. The origin and diversification of mitochondria. *Curr. Biol.* 27:R1177–R1192.

Rogers KC, Söll D. 1995. Divergence of glutamate and glutamine aminoacylation pathways: providing the evolutionary rationale for mischarging. *J. Mol. Evol.* 40:476–481.

Rugen N, Straube H, Franken LE, Braun H-P, Eubel H. 2019. Complexome profiling reveals association of PPR proteins with ribosomes in the mitochondria of plants. *Mol. Cell. Proteomics* 18:1345–1362.

Salinas-Giegé T, Giegé R, Giegé P. 2015. tRNA biology in mitochondria. *Int. J. Mol. Sci.* 16:4518–4559.

Skaltsogiannis V, Nguyen T-T, Corre N, Pflieger D, Blevins T, Hashem Y, Giegé P, Waltz F. 2024. Structural insights into maturation and translation of a plant mitoribosome. *bioRxiv* [Internet]. Available from: http://dx.doi.org/10.1101/2024.10.28.620559

Skippington E, Barkman TJ, Rice DW, Palmer JD. 2015. Miniaturized mitogenome of the parasitic plant Viscum scurruloideum is extremely divergent and dynamic and has lost all nad genes. *Proceedings of the National Academy of Sciences* [Internet] In Press. Available from: http://dx.doi.org/10.1073/pnas.1504491112 [doi]

Sloan DB, Alverson AJ, Chuckalovcak JP, Wu M, McCauley DE, Palmer JD, Taylor DR. 2012. Rapid evolution of enormous, multichromosomal genomes in flowering plant mitochondria with exceptionally high mutation rates. *PLoS Biol.* 10:e1001241.

Sloan DB, Alverson AJ, Wu M, Palmer JD, Taylor DR. 2012. Recent acceleration of plastid sequence and structural evolution coincides with extreme mitochondrial divergence in the angiosperm genus Silene. *Genome Biol. Evol.* 4:294–306.

Sloan DB, Triant DA, Forrester NJ, Bergner LM, Wu M, Taylor DR. 2014. A recurring syndrome of accelerated plastid genome evolution in the angiosperm tribe Sileneae (Caryophyllaceae). *Mol. Phylogenet. Evol.* 72:82–89.

Sloan DB, Warren JM, Williams AM, Kuster SA, Forsythe ES. 2023. Incompatibility and interchangeability in molecular evolution. *Genome Biol. Evol.* 15:evac184.

Sloan DB, Warren JM, Williams AM, Wu Z, Abdel-Ghany SE, Chicco AJ, Havird JC. 2018. Cytonuclear integration and co-evolution. *Nat. Rev. Genet.* 19:635–648.

Smith D, Asmail S. 2014. Next-generation sequencing data suggest that certain nonphotosynthetic green plants have lost their plastid genomes. *New Phytol.* 204:7–11.

Souciet G, Menand B, Ovesna J, Cosset A, Dietrich A, Wintz H. 1999. Characterization of two bifunctional Arabdopsis thaliana genes coding for mitochondrial and cytosolic forms of valyl-tRNA synthetase and threonyl-tRNA synthetase by alternative use of two in-frame AUGs: A. thalianagene characterization using two in-frame AUGs. *Eur. J. Biochem.* 266:848–854.

Steinmetz A, Weil J. 1986. Isolation and characterization of chloroplast and cytoplasmic transfer RNAs. *Methods in Enzymology* 118:212–231.

Stupar RM, Lilly JW, Town CD, Cheng Z, Kaul S, Buell CR, Jiang J. 2001. Complex mtDNA constitutes an approximate 620-kb insertion on Arabidopsis thaliana chromosome 2: implication of potential sequencing errors caused by large-unit repeats. *Proc. Natl. Acad. Sci. U. S. A.* 98:5099–5103.

Su H-J, Barkman TJ, Hao W, Jones SS, Naumann J, Skippington E, Wafula EK, Hu J-M, Palmer JD, DePamphilis CW. 2019. Novel genetic code and record-setting AT-richness in the highly reduced plastid genome of the holoparasitic plant Balanophora. *Proceedings of the National Academy of Sciences* 116:934–943.

Suzuki T, Miyauchi K. 2010. Discovery and characterization of tRNAIle lysidine synthetase (TilS). *FEBS Lett.* 584:272–277.

Timmis JN, Ayliffe MA, Huang CY, Martin W. 2004. Endosymbiotic gene transfer: Organelle genomes forge eukaryotic chromosomes. *Nat. Rev. Genet.* 5:123–135.

Uwer U, Willmitzer L, Altmann T. 1998. Inactivation of a glycyl-tRNA synthetase leads to an arrest in plant embryo development. *Plant Cell* 10:1277–1294.

Waltz F, Nguyen TT, Arrivé M, Bochler A, Chicher J, Hammann P, Kuhn L, Quadrado M, Mireau H, Hashem Y. 2019. Small is big in Arabidopsis mitochondrial ribosome. *Nature Plants* 5:106–117.

Waltz F, Soufari H, Bochler A, Giegé P, Hashem Y. 2020. Cryo-EM structure of the RNA-rich plant mitochondrial ribosome. *Nat. Plants* 6:377–383.

Warren JM, Broz AK, Martinez-Hottovy A, Elowsky C, Christensen AC, Sloan DB. 2023. Rewiring of aminoacyl-tRNA synthetase localization and interactions in plants with extensive mitochondrial tRNA gene loss. *Mol. Biol. Evol.* 40:msad163.

Warren JM, Salinas-Giegé T, Triant DA, Taylor DR, Drouard L, Sloan DB. 2021. Rapid shifts in mitochondrial tRNA import in a plant lineage with extensive mitochondrial tRNA gene loss. *Mol. Biol. Evol.* 38:5735–5751.

Warren JM, Sloan DB. 2020. Interchangeable parts: The evolutionarily dynamic tRNA population in plant mitochondria. *Mitochondrion* 52:144–156.

van Wijk KJ, Bentolila S, Leppert T, Sun Q, Sun Z, Mendoza L, Li M, Deutsch EW. 2024. Detection and editing of the updated Arabidopsis plastid- and mitochondrial-encoded proteomes through PeptideAtlas. *Plant Physiol.* 194:1411–1430.

van Wijk KJ, Leppert T, Sun Q, Boguraev SS, Sun Z, Mendoza L, Deutsch EW. 2021. The Arabidopsis PeptideAtlas: Harnessing worldwide proteomics data to create a comprehensive community proteomics resource. *Plant Cell* 33:3421–3453.

van Wijk KJ, Peltier JB, Giacomelli L. 2007. Isolation of chloroplast proteins from *Arabidopsis thaliana* for proteome analysis. *Methods Mol. Biol.* 355:43–48.

Yu R, Zhi X, Ceriotti LF, Skippington E, Rice DW, Su H-J, Barkman TJ, Sun C, Liu Y, Fang D, et al. 2025. A record-setting mitogenome in the holoparasitic plant Balanophora yakushimensis accompanied by exceptional loss of organellar DNA repair and recombination genes. *BMC Biol* [Internet] 23. Available from: http://dx.doi.org/10.1186/s12915-025-02449-8